DOI: 10.61782/fa.2023.0354

forum acusticum 2023

NUMERICAL SIMULATION OF PIEZOELECTRIC SIGNALS IN CANCELLOUS BONE USING AN FINITE-DIFFERENCE TIME-DOMAIN METHOD

Atsushi Hosokawa[1*]
[1] Department of Electrical and Computer Engineering, National Institute of Technology, Akashi College, Japan

ABSTRACT

Bone is a piezoelectric material, and the piezoelectricity is associated with bone formation. However, the piezoelectric properties in bone at ultrasound frequencies, which will lead to more efficient fracture healing by ultrasound irradiation, are not well understood. In particular, the piezoelectric properties in cancellous bone with a complicated porous trabecular structure are expected to be very complex. In this study, the piezoelectric signals generated in cancellous bone by ultrasound irradiation were numerically simulated to find out the properties. The simulation was performed using a piezoelectric finite-difference time-domain (FDTD) method, which includes piezoelectric constitutive equations in an elastic FDTD method to simulate ultrasound behaviors. The cancellous bone models were reconstructed from the microcomputed tomographic images, and the trabecular microstructures were regularly changed using an image processing technique. The correlation coefficients between the piezoelectric signal amplitude and several structural parameters were derived to investigate the structural dependences of the signal. In both cases of the ultrasound irradiations in the parallel and perpendicular directions to the major trabecular orientation, it was shown that the piezoelectric signal in cancellous bone was associated with the trabecular length in the perpendicular direction.

Keywords: *FDTD method, piezoelectric signal, cancellous bone, ultrasound*

[*] ***Corresponding author***: *hosokawa@akashi.ac.jp.*
Copyright: *©2023 Hosokawa. This is an open-access article distributed under the terms of the Creative Commons Attribution 3.0 Unported License, which permits unrestricted use, distribution, and reproduction in any medium, provided the original author and source are credited.*

1. INTRODUCTION

In recent years, low-intensity pulsed ultrasound (LIPUS) at a few megahertz (MHz) frequencies has been applied to the medical healing of bone fracture [1,2], which is based on the fact that mechanical loads can drive bone formation [3]. Bone can behave as a piezoelectric material [4], and the piezoelectric effects are considered to accompany the bone formation [5]. Many studies on the piezoelectric properties in cortical bone below a few kilohertz frequencies have been reported for more than half a century [4,6,7], and those at MHz frequencies have been also reported for the last ten years [8-13]. However, there are only a few reports of the piezoelectric properties in cancellous bone [14-16]. As cancellous bone has a complicated porous structure, it is expected that the piezoelectric properties are too complex to easily clarify. In such a case, numerical simulations, in which difficult observations in the experiments can easily performed, can be helpful. Compared with other simulation methods, a finite-difference time-domain (FDTD) method can easily model a target with complex structure such as cancellous bone. The elastic FDTD method [17] with realistic bone models reconstructed from the microcomputed tomographic (μCT) images has been widely used for simulating ultrasound behaviors in bone [18,19]. In the author's original study, the piezoelectric signals generated in cancellous bone by ultrasound irradiation were simulated by a piezoelectric FDTD (PE-FDTD) method [16,20], which is extended from the elastic FDTD method.

As the piezoelectric signal in cancellous bone is weak and sensitive to the trabecular structure [15], it is difficult to clarify the effect of the trabecular microstructure in detail. In the previous study [21], the ultrasound signals propagated through cancellous bone were simulated using the bone models in which the trabecular elements were

artificially (regularly) eroded by an image processing technique and the variability in the ultrasound properties induced by the trabecular microstructure were investigated. In the present study, the bone models with regularly changed microstructures were used in the PE-FDTD simulations in order to investigate the effect of the trabecular microstructure on the piezoelectric signal.

2. METHODS

2.1 PE-FDTD method

The PE-FDTD method is the elastic FDTD method with piezoelectric constitutive equations. The governing equations of the PE-FDTD method are given as [16,20]

$$\rho \frac{\partial \dot{u}_i}{\partial t} = \frac{\partial \tau_{ii}}{\partial x_i} + \frac{\partial \tau_{ij}}{\partial x_j} + \frac{\partial \tau_{ik}}{\partial x_k} \tag{1}$$

$$\frac{\partial \tau_{ii}}{\partial t} = (\lambda + 2\mu)\frac{\partial \dot{u}_i}{\partial x_i} + \lambda \frac{\partial \dot{u}_j}{\partial x_j} + \lambda \frac{\partial \dot{u}_k}{\partial x_k} - e_{ii}\frac{\partial E_i}{\partial t} - e_{ji}\frac{\partial E_j}{\partial t} - e_{ki}\frac{\partial E_k}{\partial t} \tag{2}$$

$$\frac{\partial \tau_{jk}}{\partial t} = \mu\left(\frac{\partial \dot{u}_j}{\partial x_k} + \frac{\partial \dot{u}_k}{\partial x_j}\right) - e_{il}\frac{\partial E_i}{\partial t} - e_{jl}\frac{\partial E_j}{\partial t} - e_{kl}\frac{\partial E_k}{\partial t} \tag{3}$$

$$\varepsilon_{ii}\frac{\partial E_i}{\partial t} = -e_{ii}\frac{\partial \dot{u}_i}{\partial x_i} - e_{ij}\frac{\partial \dot{u}_j}{\partial x_j} - e_{ik}\frac{\partial \dot{u}_k}{\partial x_k} - \frac{e_{il}}{2}\left(\frac{\partial \dot{u}_j}{\partial x_k} + \frac{\partial \dot{u}_k}{\partial x_j}\right) - \frac{e_{im}}{2}\left(\frac{\partial \dot{u}_k}{\partial x_i} + \frac{\partial \dot{u}_i}{\partial x_k}\right) - \frac{e_{in}}{2}\left(\frac{\partial \dot{u}_i}{\partial x_j} + \frac{\partial \dot{u}_j}{\partial x_i}\right) + \frac{\partial D_i}{\partial t} \tag{4}$$

$$\frac{\partial D_i}{\partial t} = -\sigma_i E_i \tag{5}$$

Here, i, j, k = 1, 2, 3, and l, m, n = 4, 5, 6. In Eqs. (1)–(5), $\dot{u}_i$ is the particle velocity in the i-direction, τ_{ii} is the normal stress in the i-direction, τ_{jk} ($j \neq k$) is the shear stress on the j–k plane, E_i is the electric field, and D_i is the electric displacement. ρ is the density, λ and μ are the first and second Lamé coefficients, respectively, e_{ij} (containing $i = j$) is the piezoelectric constant, ε_{ii} is the dielectric constant, and σ_i is the conductivity. In the PE-FDTD algorism, the spatially and temporally discretized values of $\dot{u}_i$ and D_i, and the values of τ_{ii}, τ_{ij}, and E_i are alternatively updated.

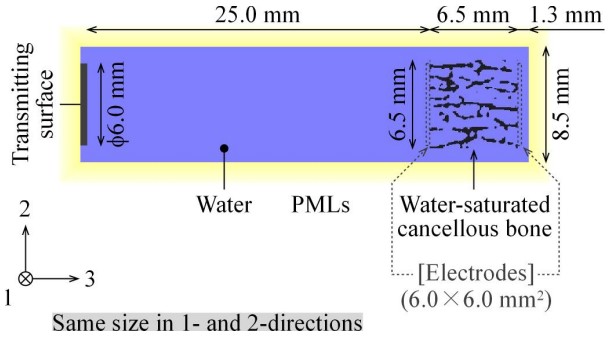

Figure 1. Numerical model for simulating piezoelectric signals generated in cancellous bone by ultrasound irradiation.

2.2 Simulation method

A cubic cancellous bone model with a side of 6.5 mm was reconstructed from the X-ray μCT image of bovine bone. It was assumed that the pore spaces were saturated with water instead of bone marrow. Three orthogonal directions in the cancellous bone model are named as $x1$-, $x2$-, and $x3$-directions in order of strong orientation of the trabecular elements. Using the image processing technique in the previous study [21], the trabecular elements in the cancellous bone model were eroded. Three erosion procedures A, B, and C were used to realize distinct changes of the trabecular microstructure with increasing porosity. In the procedure A, the erosions applied to the points of the trabecular elements, which is the transformations of the surface points of the trabeculae to the pore space (water), were randomly distributed in every direction. In the procedures B and C, the distributions of the erosions were weighted in the $x1$- and $x3$-directions, which were the major and minor trabecular-oriented directions, respectively. The porosity was 0.76 (76%) prior to erosion and was reduced to 0.85 or 0.86 by the erosion procedures.
Figure 1 shows the numerical model for the PE-FDTD simulations using the cubic cancellous bone models. As shown in Fig. 1, the three orthogonal directions in the simulation model are named as 1-, 2-, and 3-directions (note that these directions don't always coincide the $x1$-, $x2$-, and $x3$-directions in the cancellous bone model), and the sizes in the 1- and 2-directions are the same. The sizes of the simulation model were 8.5, 8.5, and 32.8 mm in the 1-, 2-, and 3-directions, respectively. At one end of this region filled with water, the cancellous bone model was allocated, and the square electrodes with a side of 6.0 mm were set in the center of the front and back surfaces on the 1–2 plane.

Table 1. Elastic [23,24] and piezoelectric [25-27] parameter values used in piezoelectric finite-different time-domain (PE-FDTD) simulations.

	Trabecula	Water
Density ρ (kg/m^3)	1960	1000
First Lamé coefficient λ (GPa)	14.8	2.2
Second Lamé coefficient μ (GPa)	8.3	0
Piezoelectric constants (μC/m^2)		
e_{31}, e_{32}, e_{33}	0.21	0
e_{14}, $-e_{25}$	1.32	0
e_{15}, e_{24}	0.26	0
Others	0	0
Dielectric constant ε (nF/m)	50.0	0.7

The circular ultrasound transmitting surface with a diameter of 6.0 mm was set on the 1–2 plane at the other end 25.0 mm apart from the cancellous bone model. To prevent artificial reflections, twenty grids of perfectly matched layers (PMLs) [22] were adopted at all boundaries surrounding the simulation model. The experimental data of the burst wave with a center frequency of 1 MHz, which corresponded to the ultrasound signal data transmitted from a Pb(Zr,Ti)O_3 (PZT) ultrasound transmitter, was applied to the normal stress components τ_{33} on the transmitting surface, and the ultrasound wave was transmitted in the 3-direction. To irradiate the ultrasound wave in the directions of the major and minor trabecular orientations, the $x1$- and $x3$-directions in the cancellous bone model were set to the 3-direction, respectively. The piezoelectric signal was calculated from the electric fields E_i in the trabecular elements between the electrodes. Then, the electrodes were regarded as perfect conductors, and the elastic properties were ignored. Table 1 lists the elastic [23,24] and piezoelectric [25-27] parameter values used in the PE-FDTD simulations. The spatial and temporal intervals were 60 μm and 4 ns, respectively.

3. RESULTS

3.1 Changes of trabecular structure in cancellous bone model

Figure 2 shows the changes of the trabecular structure in erosion procedures A, B, and C, in which the horizontal and

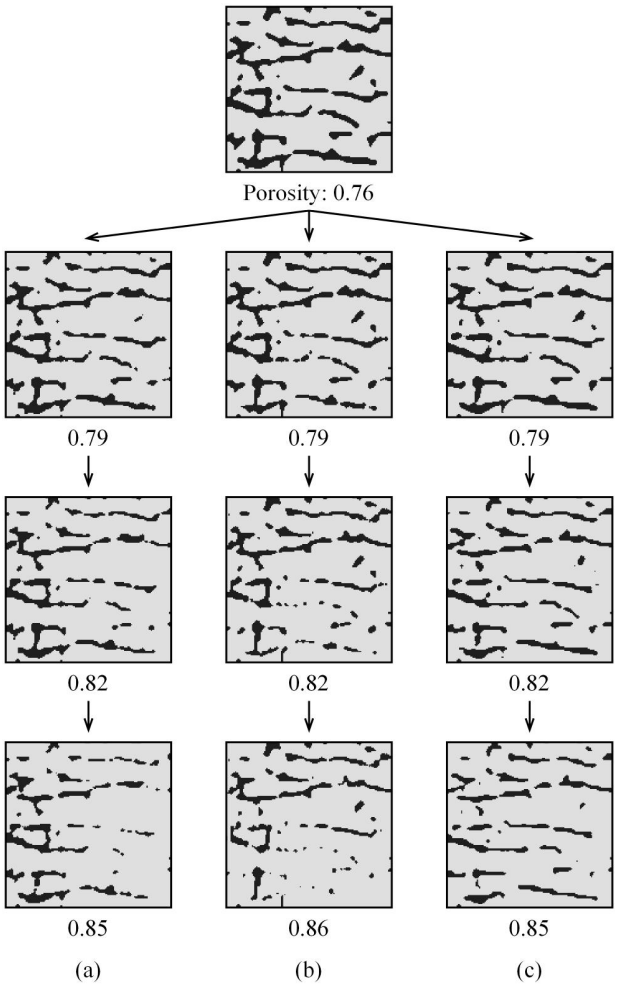

Figure 2. Changes of trabecular structure in the cancellous bone model by erosion procedures (a) A, (b) B, and (c) C.

vertical directions correspond to the $x1$- and $x3$-directions (or the major and minor trabecular-oriented directions), respectively. As shown in Fig. 2, it appears that more trabecular elements in the horizontal direction are eroded in the erosion procedure B than in the erosion procedure A, whereas more elements in the vertical direction are eroded in the procedure C. To quantitatively estimate the change of the trabecular microstructure, the degree of anisotropy (DA), that is the ratio of the maximum mean intercept lengths (MILs) [28] of the trabecular elements in the major oriented direction (or the $x1$-direction) to the minimum MIL in the minor oriented direction (or the $x3$-direction), was measured. Figure 3 shows the DAs for the cancellous bone models in

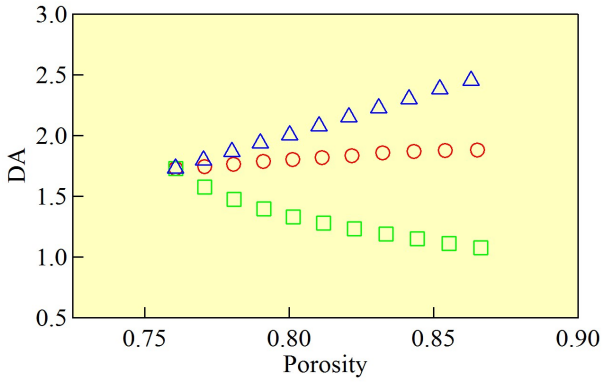

Figure 3. Variations in degree of anisotropy (DA) of the cancellous bone models with increasing porosity by erosion procedures A (circles), B (squares), and C (triangles).

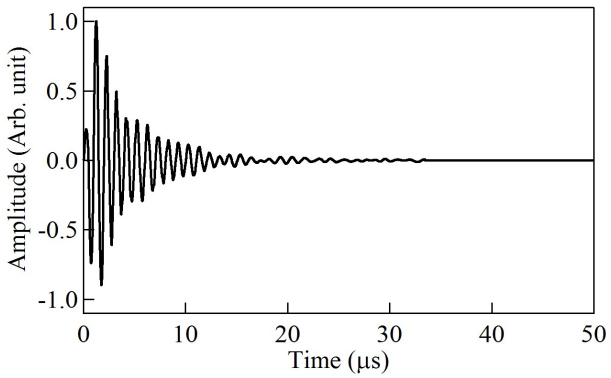

Figure 4. Waveform of irradiated ultrasound signal.

three erosion procedures, as a function of the porosity. The circular, square, and triangular marks show the DAs in the erosion procedures A, B, and C, respectively. As shown in Fig. 3, the DA scarcely varied with the porosity in the erosion procedure A, but regularly decreased and increased in the procedures B and C, respectively.

3.2 Variations in piezoelectric signal amplitude

Figure 4 shows the waveform of the irradiated ultrasound signal. Figure 5 shows the waveforms of the simulated piezoelectric signals for the water-saturated cancellous bone model before erosion; (a) and (b) show the waveforms in the cases of the ultrasound irradiations in the major and minor trabecular-oriented directions, respectively. Both piezoelectric signal waveforms in Figs. 5(a) and 5(b) were deformed from the irradiated ultrasound waveform in Fig. 4, which was due to the overlap both the ultrasound and the piezoelectric signals inside the bone [15,29]. Two piezoelectric signal waveforms were also different. The amplitude in the case of the ultrasound irradiation in the major trabecular-oriented direction was larger than that in the minor trabecular-oriented direction, which agreed with the previous experimental result [30].

Figures 6 and 7 show the amplitudes of the simulated piezoelectric signals in the cases of the ultrasound irradiations in the major and minor trabecular-oriented directions, respectively. In both figures, (a) and (b) show the amplitudes as functions of the porosity and DA, respectively, and the circular, square, and triangular marks show the amplitudes in the erosion procedures A, B, and C, respectively. In addition, the determinant coefficients of the

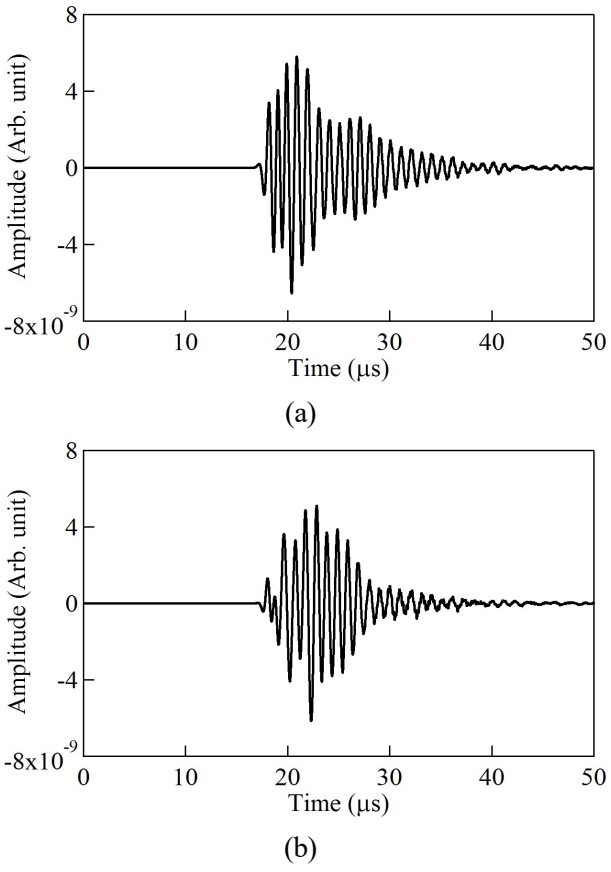

Figure 5. Waveforms of simulated piezoelectric signals in water-saturated cancellous bone before erosion in the cases of ultrasound irradiations in the (a) major and (b) minor trabecular-oriented directions.

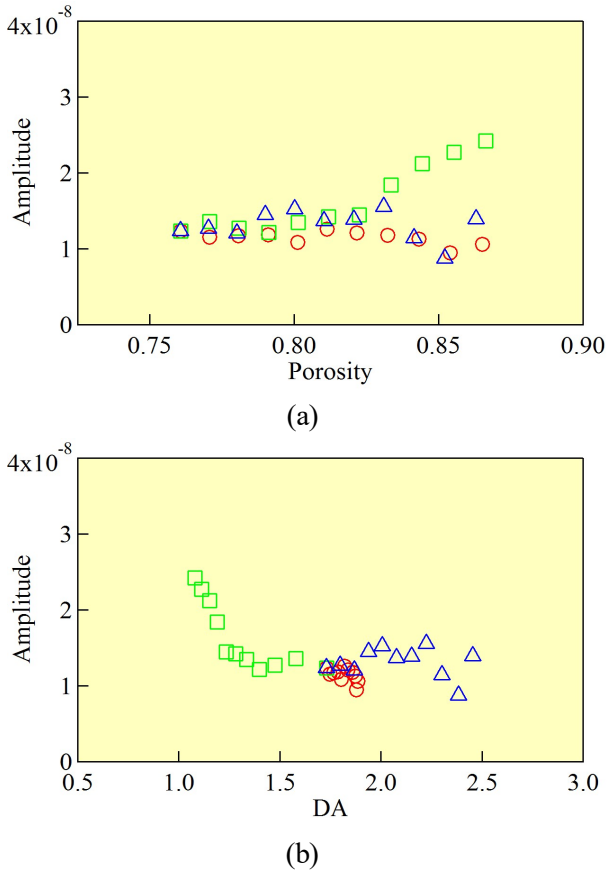

Figure 6. Variations in amplitudes of simulated piezoelectric signals with (a) porosity and (b) DA by erosion procedures A (circles), B (squares), and C (triangles) in the cases of ultrasound irradiation in the major trabecular-oriented directions.

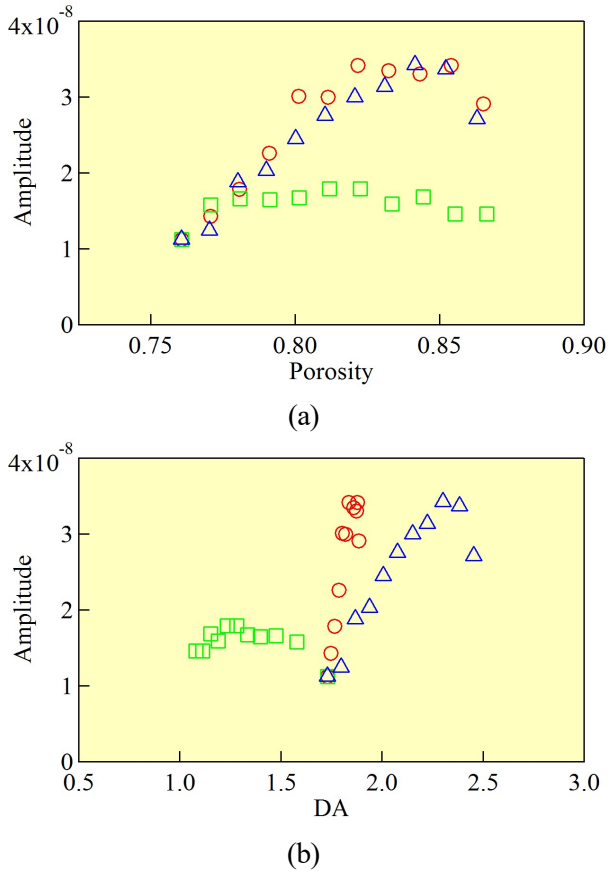

Figure 7. Variations in amplitudes of simulated piezoelectric signals with (a) porosity and (b) DA by erosion procedures A (circles), B (squares), and C (triangles) in the cases of ultrasound irradiation in the minor trabecular-oriented directions.

piezoelectric signal amplitudes with several structural parameters (porosity, DA, MILs) are listed in Tab. 3 and 4 in the cases of the ultrasound irradiations in the major and minor trabecular-oriented directions, respectively.

As shown in Figs. 6(a) and 7(a), in both cases of the ultrasound irradiations in the major and minor trabecular-oriented directions, the variations of the piezoelectric signal amplitudes in the erosion procedures A and C were similar, and these variations were different from the variation in procedure B. In the case of the ultrasound irradiation in the major trabecular-oriented direction [in Fig. 6(a)], in the erosion procedures A and C, the piezoelectric signal amplitudes didn't significantly vary with the porosity, but in the procedure B, the amplitude increased with the porosity.

In Fig. 6(b), both variation ranges of the DA and the piezoelectric signal amplitude were small in the erosion procedure A but large in the procedure B. In the procedure C, the DA variation range was large, but the amplitude variation range was small. Moreover, as shown in Tabs. 3, the piezoelectric signal amplitude was most highly correlated with the MIL in the $x3$-direction (or the minor trabecular-oriented direction) in the procedure B.

On the other hand, in the case of the ultrasound irradiation in the minor trabecular-oriented direction [in Fig. 7(a)], in the erosion procedures B, the piezoelectric signal amplitude didn't significantly vary with the porosity, but in the procedures A and C, the amplitudes increased in the porosity range of 0.76–0.85. In Fig. 7(b), in the erosion

Table 2. Determinant coefficients of piezoelectric signal amplitudes with structural parameters in the cases of ultrasound irradiation in the major trabecular-oriented directions. The $x1$- and $x3$-directions correspond to the major and minor trabecular-oriented directions, respectively.

	Procedure A	Procedure B	Procedure C
Porosity	0.35	0.83	0.02
DA	0.30	0.64	0.02
MIL in the $x1$-direction	0.30	0.63	0.00
MIL in the $x3$-direction	0.29	0.71	0.01

Table 3. Determinant coefficients of piezoelectric signal amplitudes with structural parameters in the cases of ultrasound irradiation in the minor trabecular-oriented directions. The $x1$- and $x3$-directions correspond to the major and minor trabecular-oriented directions, respectively.

	Procedure A	Procedure B	Procedure C
Porosity	0.72	0.04	0.79
DA	0.81	0.18	0.79
MIL in the $x1$-direction	0.82	0.18	0.91
MIL in the $x3$-direction	0.83	0.11	0.87

procedure A, the variation range of the DA was small, but the variation range of the piezoelectric signal amplitude was large. In the procedure B, the DA variation range was large, but the amplitude variation range was small. In the procedure C, both variation ranges were large. Moreover, as shown in Tab. 4, the piezoelectric signal amplitude was most highly correlated with the MIL in the $x1$-direction (or the major trabecular-oriented direction) in the procedure C.

4. DISCUSSION

4.1 Piezoelectric signal amplitude in ultrasound direction of major trabecular orientation

In the case of the ultrasound irradiation in the major trabecular-oriented direction, only in the erosion procedure B, the piezoelectric signal amplitude varied (increased) with the porosity, as shown in Fig. 6(a). In the procedure B, the trabecular elements were mainly eroded in the major trabecular-oriented direction, and therefore, the MIL in the minor trabecular-oriented direction increased (relative to the MIL in the major trabecular-oriented direction), as shown in the variation of the DA (Fig. 3). Moreover, the minor trabecular-oriented direction corresponded to the direction perpendicular to the ultrasound irradiation. It was therefore considered that the piezoelectric signal amplitude could increase with the trabecular length (or area) in the perpendicular direction, or the generation of the piezoelectric signal could be associated with the trabecular area in the perpendicular direction. However, when the porosity was small between 0.76 and 0.82 (or the erosion of the trabecular elements little progressed), the piezoelectric signal amplitude in the erosion procedure B didn't significantly increase with the porosity, which was similar with the amplitude variations in the procedures A and C. This was considered to be because the erosion cutting off the trabecular elements by which the trabecular area in the perpendicular direction increased was not sufficiently done in the small porosity range. Moreover, the piezoelectric signal amplitude decreased with the DA in the erosion procedure B but didn't significantly vary in the procedure C, as shown in Fig. 6(b). This also meant that the piezoelectric signal could be largely associated with the trabecular elements perpendicular to the ultrasound irradiation rather than the elements in the parallel direction.

In the other simulated results when the ultrasound wave with the longer duration time (or the larger burst cycles) was irradiated in the major trabecular-oriented direction, it was shown that all piezoelectric signal amplitudes in three erosion procedures randomly varied with the porosity, and there was not significant difference among these amplitude variations. The difference from the results in this paper was because of the longer ultrasound duration time. Owing to the porous trabecular structure in cancellous bone, the reflection, refraction, and scattering of the ultrasound signal can be caused inside the bone [14,15]. It was also shown that the piezoelectric signals could be generated at the local trabecular elements [29]. When the duration time is long, these signals can largely overlap, which can disturbance their properties.

4.2 Piezoelectric signal amplitude in ultrasound direction of minor trabecular orientation

In the case of the ultrasound irradiation in the minor trabecular-oriented direction, in the erosion procedures A

and C, the piezoelectric signal amplitude increased with the porosity until 0.84, as shown in Fig. 7(a). In the procedures A and C, the trabecular elements were eroded in the minor trabecular-oriented direction, although the erosion in the major trabecular-oriented direction was also done in the procedure A. Moreover, the major trabecular-oriented direction corresponded to the direction perpendicular to the ultrasound irradiation. Similarly with the case of the ultrasound irradiation in the major trabecular oriented direction in Sec. 4.1, it was considered that the piezoelectric signal amplitude could increase with the trabecular length (or area) perpendicular to the ultrasound irradiation, or the generation of the piezoelectric signal could be associated with the trabecular area in the perpendicular direction. However, when the porosity became large more than 0.84 (or the trabecular erosion was sufficiently progressed), the piezoelectric signal amplitudes in the erosion procedures A and C decreased with the porosity. This was considered to be because the trabecular area in the perpendicular direction decreased with the progress of erosion in the large porosity range. Moreover, the piezoelectric signal amplitude varied with the DA in the erosion procedure C but regardless of the DA in the procedure A, as shown in Fig. 7(b). This also meant that the piezoelectric signal could be associated with largely the trabecular elements perpendicular to the ultrasound irradiation, which was also similar with the case of the ultrasound irradiation in the major trabecular-oriented direction.

4.3 Relationships of piezoelectric signal amplitudes with structural parameters

Combined the discussions in Secs. 4.1 and 4.2, regardless of the ultrasound direction, the piezoelectric signal could depend on the trabecular length (or area) perpendicular to the ultrasound irradiation. In fact, as shown in Tabs. 2 and 3, both piezoelectric signal amplitudes in the major and minor trabecular-oriented directions was most highly correlated with the MILs in the minor and major directions, respectively. In other words, the piezoelectric signal amplitude was highly correlated with the trabecular length perpendicular to the the ultrasound irradiation.

5. CONCLUSIONS

The piezoelectric signals in water-saturated cancellous bone generated by ultrasound irradiation were simulated using the PE-FDTD method with the bone models in which the trabecular elements were regularly eroded, and the effect of the trabecular microstructure was investigated. In the case of the ultrasound irradiation in the major trabecular-oriented direction, the piezoelectric signal amplitude increased with the porosity by eroding the trabecular elements in the major trabecular direction. In the case of the ultrasound irradiation in the minor trabecular-oriented direction, the piezoelectric signal amplitude increased with the porosity by eroding the trabecular elements in the minor trabecular direction. These results meant that, the piezoelectric signal amplitude could increase with the trabecular length (or area) perpendicular to the ultrasound irradiation, or the piezoelectric signal could be affected by the trabecular elements in the perpendicular direction.

6. ACKNOWLEDGMENTS

This study was supported by JSPS KAKENHI Grant Number 17K06479.

7. REFERENCES

[1] L. R. Duarte, “The stimulation of bone growth by ultrasound,” *Arch. Orthop. Trauma Surg.*, vol. 101, pp. 153–159, 1983.

[2] S. Mitragotri, “Healing sound: The use of ultrasound in drug delivery and other therapeutic applications,” *Nat. Rev. Drug Discovery*, vol. 4, pp. 255–260, 2005.

[3] A. M. Parfitt, “Osteonal and hemi-osteonal remodeling: The spatial and temporal framework for signal traffic in adult human bone,” *J. Cell. Biochem.*, vol. 55, no. 3, pp. 273–286, 1994.

[4] E. Fukada and I. Yasuda, “On the piezoelectric effect of bone,” *J. Phys. Soc. Jpn.*, vol. 12, no. 10, pp. 1158–1162, 1957.

[5] M. H. Shamos and L. S. Lavine, “Physical bases for bioelectric effects in mineralized tissues,” *Clin. Orthp.*, vol. 35, pp. 177–188, 1964.

[6] C. A. L. Bassett and R. O. Becker, “Generation of electric potentials by bone in response to mechanical stress,” *Science*, vol. 137, no. 3535, pp. 1063–1064, 1962.

[7] M. H. Shamos, L. S. Lavine, and M. I. Shamos, “Piezoelectric effect in bone,” *Nature* vol. 5, p. 81, 1963.

[8] K. Ikushima, S. Watanuki, and S. Komiyama, “Detection of acoustically induced electromagnetic radiation,” *Appl. Phys. Lett.*, vol. 89, no. 19, 194103, 2006.

[9] M. Okino, S. Coutelou, K. Mizuno, T. Yanagitani, and M. Matsukawa, "Electrical potentials in bone induced by ultrasound irradiation in the megahertz range," *Appl. Phys. Lett.*, vol. 103, no. 10, 103701, 2013.

[10] H. Tsuneda, S. Matsukawa, S. Takayanagi, K. Mizuno, T. Yanagitani, and M. Matsukawa, "Effects of microstructure and water on the electrical potentials in bone induced by ultrasound irradiation," *Appl. Phys. Lett.*, vol. 106, 073704, 2015.

[11] S. Matsukawa, T. Makino, S. Mori, D. Koyama, S. Takayanagi, K. Mizuno, T. Yanagitani, and M. Matsukawa, "Effect of anisotropy on stress-induced electrical potentials in bovine bone using ultrasound irradiation," *Appl. Phys. Lett.*, vol. 110, 143701, 2017.

[12] S. Mori, T. Makino, D. Koyama, S. Takayanagi, T. Yanagitani, and M. Matsukawa, "Ultrasonically-induced electrical potentials in demineralized bovine cortical bone," *AIP Advances*, vol. 8, 045007, 2018.

[13] M. Matsukawa, "Bone ultrasound," *Jpn. J. Appl. Phys.* vol. 58, SG0802, 2019.

[14] A. Hosokawa, "Experimental observation of piezoelectric effect in cancellous bone generated by ultrasound irradiation ," *J. Acoust. Soc. Am.*, vol. 140, no. 5, pp. EL441–EL445, 2016.

[15] A. Hosokawa, "Structural dependence of piezoelectric signal in cancellous bone at an ultrasound frequency," *Proc. Mtgs. Acoust.* vol. 32, 020001, 2017.

[16] A. Hosokawa, "Effect of pore fluid on piezoelectric signal in cancellous bone generated by ultrasound irradiation," in *Proc. 2021 IEEE UFFC Latin America Ultrasonics Symposium*, pp. 1–4, 2021.

[17] J. Virieux, "P-SV wave propagation in heterogeneous media: Velocity-stress finite-difference method," *Geophysics*, vol. 51, pp. 889–901, 1986.

[18] J. J. Kaufman, G. Luo, and R. S. Siffert, "Ultrasound simulation in bone," *IEEE Trans. Ultrason. Ferroelectr. Freq. Control*, vol. 55, no. 6, pp. 1205–1218, 2008.

[19] E. Bossy and Q. Grimal, "Numerical methods for ultrasonic bone characterization," in *Bone Quantitative Ultrasound*, (Springer, Heidelberg), pp. 118–228, 2011.

[20] A. Hosokawa, "Piezoelectric finite-difference time-domain simulation of piezoelectric signals generated in cancellous bone by ultrasound irradiation," *Proc. Mtgs. Acoust.* vol. 50, 020001, 2023.

[21] A. Hosokawa, "Numerical analysis of variability in ultrasound propagation properties induced by trabecular microstructure in cancellous bone," *IEEE Trans. Ultrason. Ferroelectr. Freq. Control*, vol. 56, no. 4, pp. 738–747, 2009.

[22] W. C. Chew and Q. H. Liu, "Perfectly matched layer for elastodynamics: A new absorbing boundary condition," *J. Comput. Acoust.* vol. 4, no. 4, pp. 341–359, 1996.

[23] S. B. Lang, "Ultrasonic method for measuring elastic coefficients of bone and results on fresh and dried bovine bones," *IEEE Trans. Biomed. Eng.*, vol. 17, pp. 101–105, 1970.

[24] J. L. Williams and W. J. H. Johnson, "Elastic constants of composites formed from PMMA bone cement and anisotropic bovine tibial cancellous bone," *J. Biomech.* vol. 22, pp. 673–682, 1989.

[25] E. Fukada and I. Yasuda, "Piezoelectric effects in collagen," *Jpn. J. Appl. Phys.*, vol. 3, no. 2, pp. 117–121, 1964.

[26] S. Saha and P. A. Williams, "Electric and dielectric properties of wet human cortical bone as a function of frequency," *IEEE Trans. Biomed. Eng.*, vol. 39, pp. 1298–1304, 1992.

[27] P. A. Williams and S. Saha, "The electrical and dielectric properties of human bone tissue and their relationship with density and bone mineral content," *Ann. Biomed. Eng.*, vol. 24, pp. 222–233, 1996.

[28] W. J. Whitehouse, "The quantitative morphology of anisotropic trabecular bone," *J. Microsc.*, vol. 101, pp. 153–168, 1974.

[29] A. Hosokawa, in *Abstr. 23rd Int. Work. Quantitative Musculoskeletal Imaging with 9th Int. Symp. Ultrasonic Characterization of Bone*, p. 12, 2022.

[30] A. Hosokawa, "Piezoelectric anisotropy in water-saturated cancellous bone at an ultrasound frequency," in *Proc. e-Forum Acusticum 2020*, pp. 2695–2698, 2020.